Inelastic High-Energy Proton-Proton Collisions*

C. W. AKERLOF, D. G. CRABB,† J. L. DAY,‡ N. P. JOHNSON, P. KALBACI, A. D. KRISCH, M. T. LIN,§ M. L. MARSHAK,‖ J. K. RANDOLPH,** AND P. SCHMUESER††

Harrison M. Randall Laboratory of Physics, University of Michigan, Ann Arbor, Michigan 48104

AND

A. L. READ

National Accelerator Laboratory, Batavia, Illinois 60510

AND

K. W. EDWARDS‡‡

Department of Physics, University of Iowa, Iowa City, Iowa 52240

AND

J. G. ASBURY, G. J. MARMER, AND L. G. RATNER

Argonne National Laboratory, Argonne, Illinois 60439

(Received 21 August 1970)

We have measured the differential production cross section $d^2\sigma/d\Omega dp$ for pions, kaons, protons, and antiprotons produced in 12.4–12.5-GeV/c proton-proton collisions. We systematically studied the dependence of these cross sections on the center-of-mass longitudinal and transverse momentum of π's, K's, and $\bar{p}$'s, and on $p_{\text{c.m.}}$ and $\theta_{\text{c.m.}}$ for protons, over much of the available phase space. The extracted proton beam of the Argonne zero-gradient synchrotron (ZGS) impinged on a liquid-hydrogen target. The scattered particles were detected by a spectrometer using magnets and scintillation and Cherenkov counters to identify and momentum-analyze these particles. A steering magnet allowed detection of particles produced at different laboratory angles without moving any of the apparatus. The incident proton intensity was determined by monitor counters calibrated using foil spallation techniques. The pion production cross section was well represented by a sum of two Gaussians in $p_\perp{}^2$: $d^2\sigma/d\Omega dp = Ae^{-15p_\perp{}^2} + Be^{-3p_\perp{}^2}$. The slope for large-momentum-transfer kaon production was also about 3 (GeV/c)$^{-2}$. The pion production cross section as a function of $p_l{}^{\text{c.m.}}$ had a maximum at $p_l{}^{\text{c.m.}}=0$, possibly supporting a one-center model. Incorrect earlier measurements supporting a two-center model are discussed and corrected. The inelastic scattering cross section for protons also shows a less prominent forward peak and an $e^{-3p_\perp{}^2}$ dependence. This proton cross section also seems independent of inelasticity over a large range.

I. INTRODUCTION

THE study of proton-proton scattering has proven a fertile field for investigating strong interactions. Experimental technique has permitted numerous high-precision measurements of elastic scattering, which have placed stringent limitations on theoretical models. Many experiments have also measured pp inelastic scattering, which accounts for approximately three-fourths of the total cross section at high energy. As yet these measurements have not provided much insight into the mechanism of strong interactions. Much of the difficulty in obtaining theoretically useful results from inelastic scattering experiments stems from the ambiguities about which cross section to measure and which parameters should be independent variables. For elastic scattering, there are only a singly-differential cross section ($d\sigma/d\Omega$ or $d\sigma/dt$) and two parameters which completely specify the scattering process (p_0 and θ or $p_\perp{}^2$). For an inelastic scattering with an n-particle final state, the reaction is in general described by a very complicated differential cross section, which is a function of many parameters. Measuring such a cross section and drawing any simple insights from the data are both clearly difficult tasks. Many of the inelastic scattering experiments thus have been of the "beam-survey" type, where the doubly-differential cross section $d^2\sigma/d\Omega dp$ for the production (or scattering) of a single particle [π, K, $\bar{p}$ (or p)] is measured as a function of the incident momentum and the laboratory angle and momentum of the outgoing particle.[1] The results of these experiments

* Work supported by the U. S. Atomic Energy Commission.

† Present address: Department of Physics, St. Louis University, St. Louis, Mo. 63103.

‡ Present address: Department of Physics, University of Pennsylvania, Philadelphia, Pa. 19104.

§ Present address: Department of Physics, Michigan State University, East Lansing, Mich. 48823.

‖ Present address: School of Physics, University of Minnesota, Minneapolis, Minn. 66455.

** Present address: Department of Physics, Haverford College, Haverford, Pa. 19041.

†† Present address: Department of Physics, University of Hamburg, 2000 Hamburg-50, West Germany.

‡‡ Present address: Department of Physics, Carleton University, Ottawa, Canada.

[1] Some inelastic experiments are W. F. Baker, R. L. Cool, E. W. Jenkins, T. F. Kycia, S. J. Lindenbaum, W. A. Love, D. Luers, J. A. Niederer, S. Ozaki, A. L. Read, J. J. Russell, and L. C. L. Yuan, Phys. Rev. Letters **7**, 101 (1961); A. N. Diddens, W. Galbraith, E. Lillethun, G. Manning, A. G. Parham, A. E. Taylor, T. G. Walker, and A. M. Wetherell, Nuovo Cimento **31**, 961 (1964); D. Dekkers, J. A. Geibel, R. Mermod, G. Weber, T. R. Willitts, K. Winter, B. Jordan, M. Vivargent, N. M. King, and E. J. N. Wilson, Phys. Rev. **137**, B962 (1965); R. A. Lundy, T. B. Novey, D. D. Yovanovitch, and V. L. Telegdi, Phys. Rev. Letters **14**, 504 (1965); E. W. Anderson, E. J. Bleser, G. B. Collins, T. Fujii, J. Menes, F. Turkot, R. A. Carrigan, R. M. Edelstein, N. C. Hien, T. J. McMahon, and I. Nadelhaft, *ibid.* **16**, 855 (1966); **19**, 198 (1967); J. V. Allaby, M. Binon, A. N. Diddens, P. Duteil, A. Klovning, R. Meunier, J. P. Peigneux, E. J. Sacharidis, K. Schlüpmann, M. Spighel, J. P. Stroot, A. M. Thorndike, and A. M. Wetherell, in *Proceedings of the Fourteenth International Conference on High-Energy Physics, Vienna, 1968*, edited by J. Prentki and J. Steinberger (CERN, Geneva, 1968); D. B. Smith, R. J. Sprafka, and J. A. Anderson, Phys. Rev. Letters **23**, 1064 (1970).

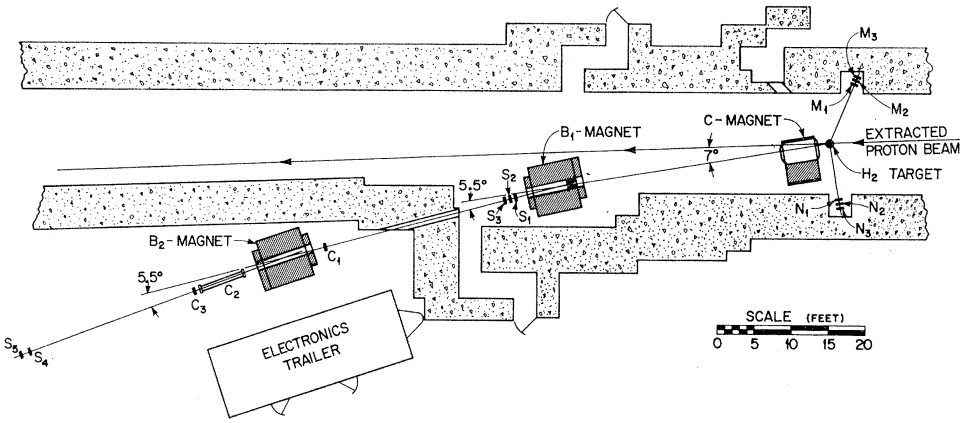

FIG. 1. Layout of experiment. Incident protons impinge on the liquid-hydrogen target and the produced particles are detected by the spectrometer.

have proven useful for the design of secondary particle beams and have provided a basis for several *ad hoc* parametrizations.[2] But there were few serious attempts to relate this data to the theory of strong interactions.[3] Several authors have attempted to parametrize the beam-survey data in terms of center-of-mass (c.m.) variables on the supposition that the interaction might be simpler in this frame of reference, but these attempts have failed to isolate a unique dependence.[4] The idea has persisted, however, that because of its symmetry the c.m. frame should be used for a systematic study of pp inelastic scattering.

Over the past three years,[5] we systematically measured production cross sections from pp collisions for several types of particles as a function of c.m. variables. We thus studied reactions such as

$$p+p\rightarrow\pi^{+}+\text{anything}, \tag{1}$$

where we detected only the outgoing pion and had no information about the other final-state particles. The cross section for this process is, of course, qualitatively different from the cross section for a single channel such as

$$p+p\rightarrow p+n+\pi^{+}. \tag{2}$$

It represents rather a summation over this single channel and every other channel in which a π^{+} is produced. Despite the qualitative difference, the summed cross section is perfectly well defined experimentally by the equation

$$\frac{d^{2}\sigma}{d\Omega dp}=\frac{\text{events}}{I_{0}N_{T}\Delta\Omega\Delta p}, \tag{3}$$

where I_0 is the incident intensity, N_T is the number of target protons per cm^2, and $\Delta\Omega\Delta p$ is the spectrometer phase-space acceptance.

For secondary particles which were not present in the initial state (π, K, and $\bar{p}$), we measured the c.m. cross section $d^2\sigma/d\Omega dp$ as a function of $p_\perp^2$, the Lorentz-invariant transverse momentum squared of the produced particle, while holding p_l, the particle's c.m. longitudinal momentum, fixed. In another series of measurements, we fixed $p_\perp^2$ and measured the dependence of the cross section on p_l.

We also measured the inelastic scattering cross section for protons in the reaction

$$p+p\rightarrow p+\text{anything}. \tag{4}$$

For this portion of the experiment we used different c.m. variables to study this process as the inelastic analog to elastic scattering. For these measurements, the c.m. momentum of the scattered proton $p_{\text{c.m.}}$ was held fixed, while $\theta_{\text{c.m.}}$ was varied.

The measurements described in this paper were made in the extracted proton beams of the Argonne zero-gradient synchrotron (ZGS) in three phases over a period of three years. All three experiments used substantially the same apparatus, but with some significant differences. The changes reflected both an improvement of the system based on knowledge gained from previous phases and a desire to cover different kinematic regions. The three sets of measurements (referred to as I, II, and III) were made in three successive years.

[2] G. Cocconi, L. J. Koester, and D. H. Perkins, LRL Report No. UCRL-10022, 1961 (unpublished); J. Ranft, CERN Report No. MPS/EP 66-4, 1966 (unpublished); G. H. Trilling, LRL Report No. UCRL-16830, 1966 (unpublished).

[3] One example is R. Hagedorn, Nuovo Cimento **52A**, 1336 (1967).

[4] The various parametrizations listed in Ref. 2 indicate the diversity obtained.

[5] As indicated in the following references, not all the authors of this paper participated in all phases of the experiment: L. G. Ratner, K. W. Edwards, C. W. Akerlof, D. G. Crabb, J. L. Day, A. D. Krisch, and M. T. Lin, Phys. Rev. **166**, 1353 (1968); Phys. Rev. Letters **18**, 1218 (1967); D. G. Crabb, J. L. Day, A. D. Krisch, M. T. Lin, M. L. Marshak, J. G. Asbury, L. G. Ratner, and A. L. Read, *ibid.* **21**, 830 (1968); J. G. Asbury, L. G. Ratner, A. L. Read, D. G. Crabb, J. L. Day, A. D. Krisch, M. T. Lin, and M. L. Marshak, *ibid.* **21**, 1097 (1968); J. L. Day, N. P. Johnson, A. D. Krisch, M. L. Marshak, J. K. Randolph, P. Schmueser, G. J. Marmer, and L. G. Ratner, *ibid.* **23**, 1055 (1969); G. J. Marmer, L. G. Ratner, J. L. Day, N. P. Johnson, P. Kalbaci, A. D. Krisch, M. L. Marshak, and J. K. Randolph, *ibid.* **23**, 1469 (1969).

II. EXPERIMENTAL METHOD

A typical experimental layout is shown in Fig. 1. The external proton beam of the ZGS impinged on a liquid-hydrogen target. The produced particle was identified and momentum-analyzed by a single-arm spectrometer consisting of bending magnets and scintillation and Cherenkov counters. This spectrometer was essentially identical to the ones used in beam-survey experiments, with the exception of the additional C magnet, located near the hydrogen target. The field in this magnet was adjusted to steer particles produced at various laboratory angles into the spectrometer. Use of the steering magnet effectively allowed the experiment to be done in the c.m. frame. One or two B magnets deflected the particles for momentum analysis. Two sets of monitor telescopes, calibrated by foil irradiation runs, determined the incident proton beam intensity.

A. Proton Beam and Monitoring

Phases I and II of the experiment were performed in the first extracted proton beam of the ZGS (EPB I) and phase III was done in EPB II. Circulating protons in the main ring of the ZGS were extracted into both beam lines using the Piccioni energy-loss system. Both beams were transported to the hydrogen targets through a set of two quadrupole doublets and several bending magnets. The quadrupoles and bending magnets were tuned according to calculations made by standard beam design computer programs. The beam spot at the hydrogen target was optimized by varying the currents in the beam transport elements and seeking a maximum number of coincidences in both monitor telescopes. During phase III, the alignment and size of the beam at the target were monitored continuously during the running of the experiment, using a segmented wire ion chamber[6] (SWIC) developed by the ZGS staff. The focus at the target depended much more sensitively on the current in the beam bending magnet than on the quadrupole currents. The final settings for the beam transport magnets were always very close to those calculated by the beam optics computer program.

For all beams used in this experiment, the tuned spot size was approximately 1 cm diam, the angular divergence was about ± 3 mrad, and the monochromaticity was better than $\pm\frac{1}{4}\%$. A complete listing of the parameters of each of the three incident beams used in the experiment is given in Table I.

The two monitor telescopes, located just upstream of the target on either side of the tunnel, each counted coincidences in proportion to the number of protons incident on the target. Using two monitor telescopes reduced systematic normalization errors and detected any gross changes in the monitor counters during the experiment. In each section of the experiment, the ratio of coincidences in the two monitor telescopes ($M:N$) varied less than 5%. The monitor counters were $\frac{1}{2}\times 1$-in. Pilot B scintillators; the axis of the three counters pointed to the hydrogen target through ports in the target casing. The number of events in each telescope was multiplied by a fixed ratio to give each side an approximately equal statistical weight in determining the incident intensity.

To obtain the ratio of incident protons to monitor counts, we had calibration runs with the hydrogen target both full and empty. A radiochemical analysis of a metal foil, which was placed just upstream of the target, determined the number of incident protons during a calibration run. The primary spallation re-

TABLE I. Incident beam parameters.

	Beam I	Beam II	Beam III
Incident momentum (GeV/c)	12.5	12.5	12.4
Uncertainty in p_0 (%)	$<\pm\frac{1}{2}$	$<\pm\frac{1}{2}$	± 1
Spot size at target (cm)	~ 1	~ 1	~ 1
Angular divergence (mrad)	± 3	± 3	± 3
Monochromaticity (%)	$<\pm\frac{1}{4}$	$<\pm\frac{1}{4}$	$<\pm\frac{1}{4}$
Spill (msec)	300	500	550
Intensity (per pulse)	$(1\text{–}2)\times 10^{11}$	$(1\text{–}5)\times 10^{11}$	2×10^{10}
Repetition rate (pulses/min)	~ 24	18–20	18–20

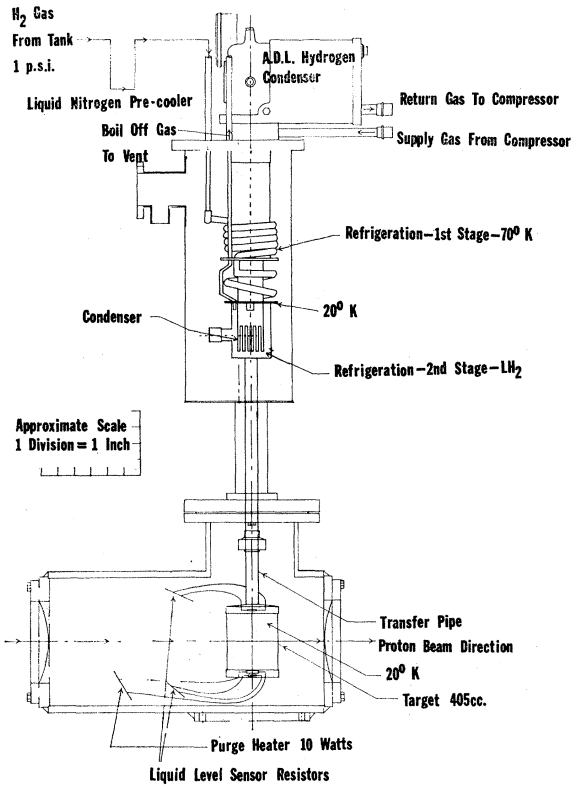

FIG. 2. Schematic diagram of the self-refrigerating liquid-hydrogen target.

[6] F. Hornstra, Jr., and J. R. Simanton, Nucl. Instr. Methods 68, 138 (1969); J. R. Simanton, R. F. Marguardt, and F. Hornstra, Jr., *ibid.* 68, 209 (1969).

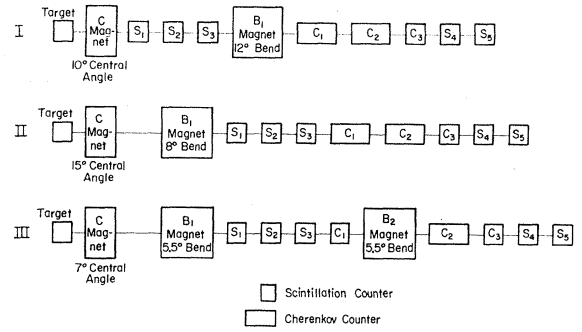

FIG. 3. Block diagram of the three spectrometers used in the different phases of the experiment.

action used was $^{197}Au \rightarrow {}^{149}Tb$ in gold foils, but as a check some runs were taken measuring the production of ^{24}Na and ^{18}F in aluminum foils. The $\pm 5\%$ uncertainty in the spallation cross section introduced an error into the over-all normalization of the data, but gave no point-to-point systematic error.[7] The results of all calibration runs using both types of foils were consistent to within $\pm 3\%$.

B. Hydrogen Target

All three phases of the experiment used a vertical, cylindrical flask of liquid hydrogen as a target. During phase I the flask was 2 in. in diameter; for phases II and III, the flask diameter was 3 in. The target flask was always made of 0.003-in. *H*-film; it was enclosed in an aluminum vacuum casing, which had 0.005-in. *H*-film entry and exit ports for the beam and the scattered particle. The flask was wrapped with several layers of 0.00025-in. aluminized Mylar superinsulation to reduce radiative heat transfer. The monitor ports on either side of the target were also 0.005-in. *H*-film. A diagram of a typical target is shown in Fig. 2.

The targets were all of the self-refrigerating type, which permitted the safe use of thin-window construction. The use of these thin windows significantly reduced the target-empty effect, which is always a large correction for single-arm spectrometer experiments. An Arthur D. Little, Inc. cryostat cooled the helium, which cooled the hydrogen gas below its boiling point, so that it condensed in the target flask. Two thermistors, one located at the top and one at the bottom of the target flask, indicated whether the target was full. In addition, a hole cut in the Mylar superinsulation permitted a visual check of the liquid level.

The target-empty correction was determined by taking otherwise identical data runs with the target flask purged of liquid hydrogen. This correction ranged from 9 to 35% depending on the momentum and angle of the produced particle. In general, the effect was smallest at the largest production angles; it was, of course, proportionately larger for the 2-in. target than for the 3-in. targets. Most of the effect came from beam interactions with the *H*-film windows, but some target-empty events came from interactions in the aluminum vacuum jacket. An estimated 1% correction was made for the solid-nitrogen frost which occasionally formed on the target flask.

C. Spectrometer

A schematic diagram of the three single-arm spectrometers used in the different phases of the experiment is shown in Fig. 3. The use of the C magnet eliminated the necessity for moving any of the apparatus to detect particles produced at different angles in the laboratory. The C magnet bent a particle with a noncentral trajectory back towards the axis of the spectrometer. The field in the first B magnet was then adjusted to bend the particle so that its trajectory passed through the remaining counters. For particles produced on the other side of the central axis, the C-magnet polarity was reversed and the field in the first B magnet was again adjusted so that the particle's path again went through the downstream counters. Thus two magnets were required to steer particles produced at various angles into the acceptance of the spectrometer—one to correct the displacement of the particle from the central axis and one to realign its trajectory. The C magnet was placed as close as possible to the target in order that the steering system cover as large an angular range as possible. For example, in phase III particles in the range $0° \rightarrow 18°$ could be returned to the spectrometer axis and detected using this arrangement.

There was a major design error in the spectrometer used in phase I of the experiment (spectrometer I), which resulted in incorrect cross sections. In that spectrometer, particles were not fully restored to the central axis before passing through the first three scintillation counters. As shown in Fig. 4, the C magnet was set to bend particles through the center of counter S_3; for large restoration angles ($|\theta_{lab} - \theta_{axis}| > 3°$),

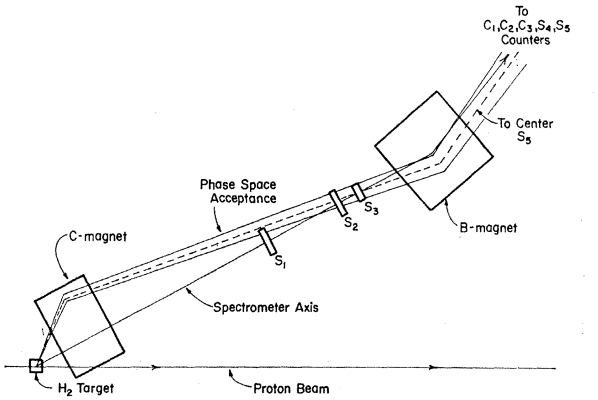

FIG. 4. Layout of spectrometer I, showing that some particles restored through large angles could miss the S_1 counter. This drawing is not to scale.

[7] J. B. Cummings, J. Hudis, A. M. Poskanzer, and S. Kaufman, Phys. Rev. **128**, 2392 (1962); J. B. Cummings, Ann. Rev. Nucl. Sci. **13**, 260 (1963).

TABLE II. Size and location of counters.

Counter	Spectrometer I Size (in.)	Spectrometer I Location (in. from target)	Spectrometer II Size (in.)	Spectrometer II Location (in. from target)	Spectrometer III Size (in.)	Spectrometer III Location (in. from target)
S_1	$1\times1\frac{1}{4}$[a]	200	$\frac{3}{4}\times1\frac{1}{2}$[a]	260	$1\frac{1}{2}\times2$[a]	510
S_2	1×1	235	$1\times1\frac{1}{2}$	$266\frac{1}{2}$	$1\frac{3}{4}\times2$	$516\frac{1}{2}$
S_3	$\frac{3}{4}\times\frac{3}{4}$[a]	240	$1\times1\frac{1}{2}$	273	$1\frac{3}{4}\times2$	523
S_4	6×6	1000	6×5	950	6×5	$1347\frac{1}{2}$
S_5	6×5[a]	1100	$6\times3\frac{1}{2}$[a]	1200	5×4[a]	1350
C_1	5 (diam) 38 (length)	730	5 (diam) 38 (length)	615	4×4	840
C_2	5 (diam) 20 (length)	760	5 (diam) 20 (length)	645	5 (diam) 72 (length)	1040
C_3	4×4	785	4×4	650	6×6	1050

[a] Defining counter. All scintillators were $\frac{1}{2}$ in. thick. Sizes given are horizontal×vertical.

counter S_1 was not sufficiently overmatched. Thus the spectrometer acceptance was not defined by S_3 and S_5 alone, as was intended. As a result, some of the previously published cross sections are in error.[8] After discovery of this effect, these data were reanalyzed using a Monte Carlo computer program to simulate the actual condition of the spectrometer. For some points there was no correction for this effect and for others the correction was small and could be made with reasonable accuracy; these corrected cross sections are tabulated in this paper. Most points with large corrections were subsequently remeasured during later stages of the experiment. Although the corrected data agrees substantially with the new data, indicating an understanding of the error in spectrometer I, only the newer data for remeasured points are given in the tables. Both the corrected and remeasured points are shown in the figures.

This phase-space definition problem did not affect spectrometers II and III. In these arrangements all counters were located downstream of the first B magnet, which completely realigned particles along the spectrometer axis. The phase-space acceptance was then defined only by scintillation counters S_1 and S_5. All other scintillation counters and the Cherenkov telescope were overmatched. The sizes of the various counters and their locations for each stage of the experiment are listed in Table II.

Since both defining counters were downstream of two bending magnets (C and B_1), the definition of p and θ was coupled. As shown in Fig. 5, the S_1 counter defined a strip in p-θ space and S_5 defined another intersecting strip. The particle in the phase space common to both strips triggered both S_1 and S_5 giving an event. Thus a parallelogram was the horizontal acceptance of the spectrometer. A standard phase-space matrix program computed the parallelogram for each data point; a typical set of parallelograms for the horizontal plane is shown in Fig. 6. The vertical acceptance was defined by S_5 alone and was approximately the height of S_5 divided by the distance from it to the target. The phase-space matrix program calculated the small correetion to the vertical acceptance resulting from vertical focusing in the bending magnets. The total phase-space acceptance of the spectrometer was the product of thc horizontal and vertical acceptances. The spectrometer phase space was typically $\Delta\Omega\Delta p=(1.5\text{–}3)\times10^{-6}$ (GeV/c) sr in the laboratory or $\Delta\Omega\Delta p|_{\text{c.m.}}=(5\text{–}10)\times10^{-6}$ (GeV/c) sr. A detailed list of the spectrometer characteristics for each stage of the experiment is given in Table III.

In phases II and III of the experiment, lead collimators were used in the spectrometer to reduce the accidentals-background and target-empty effects. These collimators were not defining for particles coming from the hydrogen target. The inner sides of the collimators were placed at least 1 in. from the edges of the spectrometer acceptance envelope to eliminate any effects from particles scattering on the collimators.

The magnetic field integrals ($\int\mathbf{B}\cdot d\mathbf{l}$) for all the magnets were measured by the ZGS staff using NMR,

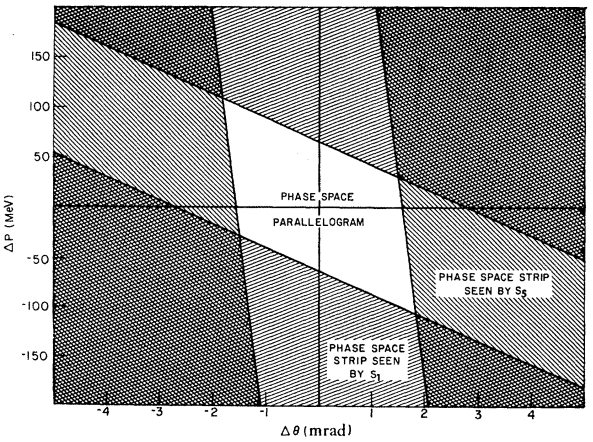

FIG. 5. Plot of the phase space $\Delta\theta\Delta p$ of the produced particles. The intersection of the two strips defined by S_1 and S_5 is the phase space subtended by the spectrometer. This particular drawing is for spectrometer I; the phase-space definition for spectrometers II and III is similar.

[8] The data listed in this paper then supersede all tables in Ratner *et al.*, Ref. 5.

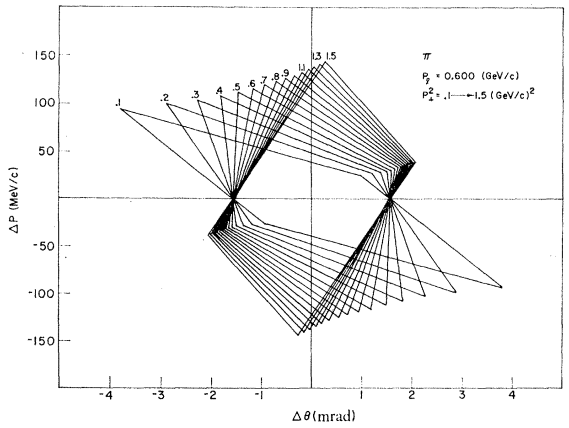

FIG. 6. Examples of the $\Delta\theta\Delta p$ parallelograms subtended by the spectrometer. This series of parallelograms corresponds to $\pi^\pm$ measurements with $p_l^{\text{c.m.}}=0.6$ GeV/c.

flip-coil, and wire-orbit techniques.[9] In setting the magnet currents a correction was made for the fact that the particular field integral along the particle trajectory was different from the field integral along the center line of the magnet. During phases I and II, the magnetic fields were set by reading the voltage produced across a standard shunt in series with each magnet power supply. The voltage was read with two digital voltmeters in parallel. In phase III the digital voltmeters measured the output of a solid-state transducer connected in series with the magnet. The shunt and transducer outputs were calibrated by NMR measurements of the magnetic fields. During one of several checks of the transducer calibration during phase III, it was discovered that the transducer output was slightly polarity dependent. This dependence resulted in no more than a 2% correction in the momentum for some of the positive particle data points. After the end of the experiment, we also discovered that both B magnets used in phase III were slightly different from previously manufactured magnets of the same series. A detailed field mapping determined that the effective length for these particular magnets was slightly longer than for other magnets of the same nominal type; in addition, the effective length was somewhat current dependent. This remeasurement of the effective length resulted in a correction to the data of phase III of not more than $(4\pm2)\%$. Also, the parameters of these data points were slightly changed; for example, $p_1^2=0.20$ (GeV/c)^2 became $p_1^2=0.22$ (GeV/c)^2.

TABLE III. Spectrometer parameters.

	Spectrometer I	Spectrometer II	Spectrometer III
Central angle (deg)	10	15	7
Maximum angle (deg)	13	20	18
Minimum angle (deg)	7	10	0
Typical $\Delta\Omega\Delta p\|_{\text{lab}}$ [(GeV/c) sr]	1.5×10^{-6}	3×10^{-6}	3×10^{-6}
Typical $\Delta\Omega\Delta p\|_{\text{c.m.}}$ [(GeV/c) sr]	5×10^{-6}	10^{-5}	10^{-5}
No. of B magnets	1	1	2
Nominal bend angle in each B magnet (deg)	12	8	5.5

[9] Argonne ZGS Users Handbook, Argonne National Laboratory (unpublished).

D. Cherenkov Counters

The Cherenkov telescope identified the particles as pions, kaons, protons, or antiprotons. In phases I and II two threshold Cherenkov counters C_1 and C_2 filled with ethane gas were used; C_3 was a scintillation counter intended to reduce the number of accidental coincidences. In phase III, only C_2 was actually a Cherenkov counter; C_1 and C_3 were scintillation counters also used to reduce accidentals. Nitrogen and ethane gas were used in the C_2 counter during phase III, depending on the velocity of the particles to be detected. When two Cherenkov counters were used (phases I and II), C_2 was always run in coincidence, while C_1 was run in anticoincidence to reject pions during the kaon data runs and to reject both pions and kaons during the measurements of antiprotons. To detect pions, C_2 was switched out of the logic circuitry. During the kaon runs, for example, the C_2 pressure was set high enough to detect only pions and kaons but not protons, while C_1 rejected pions. During phase III, C_2 was either set in coincidence to detect pions but not kaons or protons or in anticoincidence to reject pions and kaons but not protons. The appropriate gas pressures were determined experimentally by running pressure curves at several points and interpolating between them. Typical curves used to determine pressure settings for positive and negative kaons are shown in Figs. 7 and 8. The pressures determined by this method agreed well with threshold pressures calculated using the velocity of the particle and the index of refraction of the gas as a function of pressure.[10]

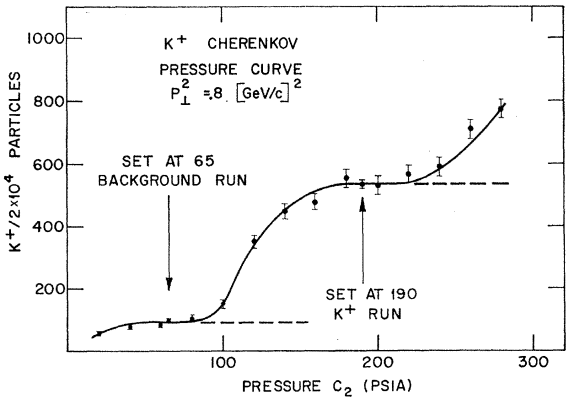

FIG. 7. Cherenkov pressure curve for K^+ mesons. Notice first the low-pressure plateau of unrejected π^+ mesons, then the K^+ plateau and the rising curve of proton events. Some proton events contaminate the K^+ plateau. Note that 14.5 PSIA equals 1 A_s.

[10] W. Galbraith, *High Energy and Nuclear Physics Handbook* (Rutherford High Energy Laboratory, England, 1964), Sec. VI.

The Cherenkov rejection efficiency was only about 0.997 so that it was necessary to determine the unrejected background for kaon and antiproton data. This subtraction was determined for K^-, for example, by setting the pressure in both Cherenkov counters such that they would detect only pions. With one Cherenkov counter in coincidence and the other in anticoincidence, the number of events was a measure of the unrejected background. For positive kaons, the rejection problem was complicated by a large background of high-momentum protons. To correct for unrejected protons, both Cherenkov counters were set on the K plateau—one in coincidence and the other in anticoincidence. The number of spectrometer coincidences measured the unrejected high-momentum-proton background. During phase I of the experiment, only pion rejection inefficiency tests, but not proton rejection tests, were made. The K^+ data from that section of the experiment thus were contaminated by a considerable proton background. For some of these points, the proton background could be unambiguously separated from the kaon events using the time-of-flight spectrum; these corrected data are listed in Table VI.[11] The K^- data were not affected by this problem and are also listed in Table VI. During phase II both pion and proton backgrounds were measured for the kaon data; in phase III no kaon or antiproton data were measured. The unrejected background subtraction for K^- data was always less than 25%. For K^+ and $\bar{p}$ data, the background subtraction was greater than 50%.

The two Cherenkov counters changed very little during the three phases of the experiment. As shown in Fig. 9, the gas was contained in an aluminum tube 5 in. in diameter. The particles entered and exited through aluminum windows which were 0.1 in. thick in phases I and II of the experiment and 0.05 in. thick in phase III. Cherenkov light was gathered by an aluminized Lucite mirror 0.125 in. thick and reflected through a UVT Lucite light pipe into the photomultiplier (Amperex 56UVP for phases I and II; RCA 8575 for phase III). Aluminized Mylar was wrapped around the inside of the aluminum tube to improve the light gathering efficiency. The particular dimensions of the Chernekov counters used in each stage of the experiment are listed in Table II.

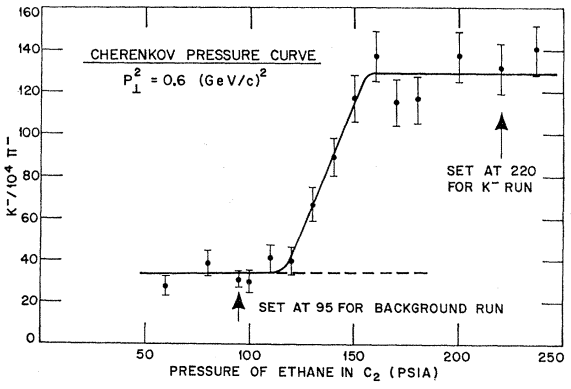

FIG. 8. Cherenkov pressure curve for K^- mesons. The high-pressure flat area is the K^- plateau; the low-pressure plateau results from unrejected pions.

[11] The K^+ cross sections listed in Ratner *et al.* (Ref. 5) and not listed here are incorrect because of unrejected proton background.

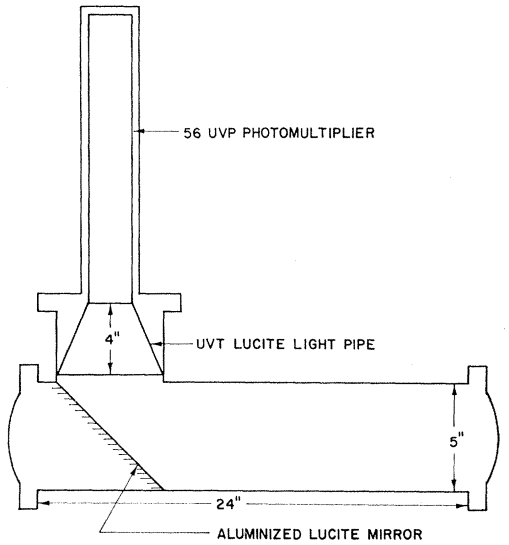

FIG. 9. Diagram of one of the threshold Cherenkov counters used in the experiment. Particles pass through the horizontal tube. The mirror reflects the Cherenkov light through the light pipe into the vertically mounted photomultiplier.

E. Electronics

The scintillation counters and the fast-logic circuitry were essentially identical in all phases of the experiment. All scintillation counters were $\frac{1}{2}$-in. Pilot B scintillators optically connected through air light pipes for S_1, S_2, and S_3 and Lucite light pipes for the remainder of the counters to RCA 7746 photomultipliers. The air light pipes made from aluminized glass tubes were used for the three counters located inside the proton tunnel to reduce the background due to Cherenkov radiation in the light pipes. The Lucite light pipes on the other counters were oriented in different directions to reduce the probability of this type of event. The photomultiplier voltages were set by running standard high-voltage plateau curves. When necessary, the time delay in each photomultiplier output cable was altered to compensate for different flight times through the spectrometers for particles of different velocity. These delays were set experimentally by running standard delay curves.

The signals from the photomultipliers were logically analyzed by Chronetics 100-mHz circuitry. The outputs of the logic network were displayed on 100-mHz TSI scalers. Important quantities were double-counted on two independent scalers. The scaler outputs were recorded at the end of each data run using a Polaroid camera. A time-of-flight spectrum for the particles

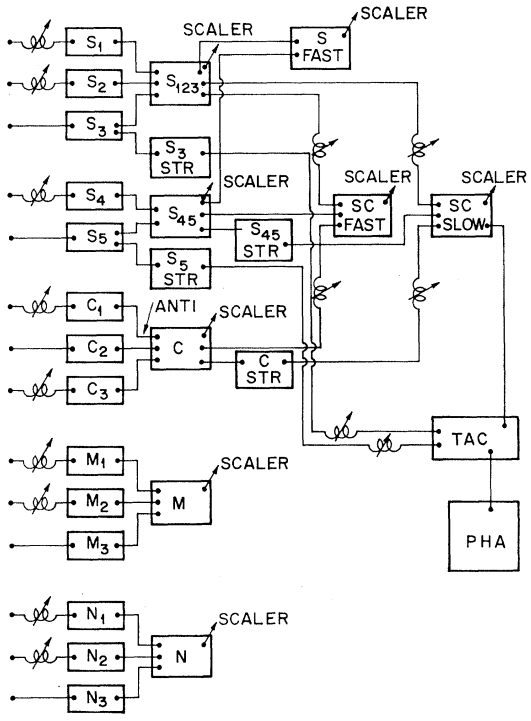

FIG. 10. Electronics block diagram for formation of SC_{slow} and SC_{fast} coincidences and for the time-of-flight analysis.

traversing the spectrometer was accumulated and displayed by a TMC 400-channel pulse-height analyzer (PHA).

The signals from each photomultiplier were fed into separate discriminators. The outputs of discriminators S_1, S_2, and S_3 formed a threefold coincidence S_{123}, as shown in the schematic diagram of the logic circuitry in Fig. 10. Similarly, the signals from counters S_4 and S_5 formed a double coincidence S_{45}. These two coincidences were combined to form an additional twofold coincidence $S_{\text{fast}}=S_{123}S_{45}$, which counted the number of charged particles passing through the spectrometer. The three counters of the C telescope formed a threefold coincidence, as has already been described, to identify the particle as a π, K, p, or $\bar{p}$. The resolving times for all these coincidences were approximately 5 nsec.

The indication of a desired inelastic scattering event was the threefold coincidence $SC_{\text{fast}}=S_{123}S_{45}C$, with a resolving time of about 5 nsec. To correct for accidental events, a second threefold coincidence SC_{slow} was formed with a resolving time of 30 nsec. Each of the three input signals to this slow coincidence were separately stretched in a discriminator. Since the resolving times for the two coincidences were known, the two quantities SC_{slow} and SC_{fast} permitted an extrapolation of the SC_{fast} coincidence rate to zero resolving time. In particular, the number of accidentals in SC_{fast} was $\frac{1}{5}(SC_{\text{slow}}-SC_{\text{fast}})$.

Another more accurate technique was used to correct the data when the number of accidentals was more than 1% of the coincidence rate. The time of flight between counters S_3 and S_5 was measured using a time-to-amplitude converter (TAC). The TAC determined the time overlap between stretched pulses from S_3 and S_5 for each SC_{slow} coincidence. The TAC output was then accumulated and displayed at the end of each run as a peak with a width of about 1.5 nsec FWHM, as shown in Fig. 11. The number of accidental coincidences was calculated from the broad background under the peak. The accidentals subtraction ranged from 1 to 15% with an uncertainty of 1–5% in phase I of the experiment; for phases II and III the proton beam intensity was lowered and the subtraction was less than 1%.

F. Experimental Tests

Throughout all phases of the experiment we performed a number of tests to check the reliability of the experimental data. Delay curves for all coincidences determined that we counted real events. Target-empty runs permitted deletion of spurious events from interactions in the target walls. High-voltage curves demonstrated that all photomultipliers were operating properly. Cherenkov pressure curves indicated that the Cherenkov counters were operating correctly and quantitatively measured the inherent inefficiencies of these counters. During phase III when there were two B magnets, we also ran B-magnet curves—varying the field in one B magnet while holding the field in the other fixed. These curves indicated that the magnetic field integrals were set properly relative to one another, as shown in Fig. 12.

As indicated later, in phase III we observed a strong forward peaking, particularly prominent in the pion production cross section. Several checks were made to determine whether this additional forward peaking was a real effect. These tests included setting the C magnet so that particles produced on the right-hand side of the spectrometer rather than the left-hand side were detected, checking the target-empty spectrum for the

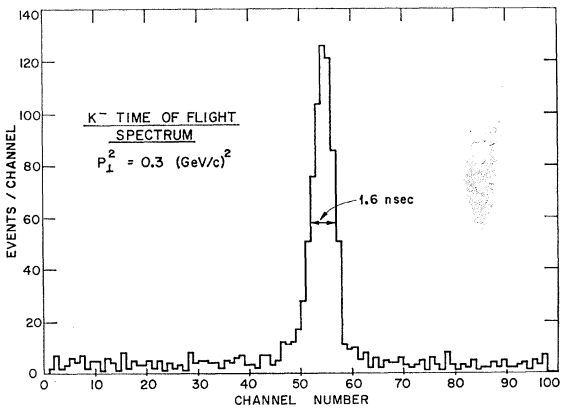

FIG. 11. Time-of-flight spectrum from the pulse-height analyzer. The number of coincidences is plotted against the time of flight between the S_3 and S_5 counters. Each channel represents about 0.4 nsec.

TABLE IV. Corrections and uncertainties.

		Phase I		Phase II		Phase III	
		Correction factor	Uncertainty (%)	Correction factor	Uncertainty (%)	Correction factor	Uncertainty (%)
Absorption	π	1.14	2	1.13	2	1.19	3
	K	1.15	2	1.13	2	...	...
	$\bar{p}$	1.30	4	...	...	...	...
	p	...	...	1.20	3	1.25	4
Decay	π	0.09–1.28	0–5	1.05–1.09	2	1.05–1.30	2–4
	K	1.93–3.4	5–10	1.98–2.13	10	...	...
Multiple Coulomb scattering		1.03–1.28	2–6	1.00	2	1.00–1.45	0–10

forward peak region and rechecking Cherenkov pressure curves for this region.

All these tests proved negative, indicating that the forward peaking is a real effect. The cross section fell very strongly on both sides of the beam axis. The target-empty spectrum showed no forward peaking, which indicated that these particles were actually produced in the liquid-hydrogen target and not someplace upstream in the proton beam line. The Cherenkov pressure curves for the forward peak region were flat over several hundred psi, indicating that there was no significant contamination from the production of electrons or muons. Slightly moving the beam spot and slightly increasing its size also had no effect on the forward peak.

III. RESULTS

A. Corrections and Experimental Errors

A number of corrections were made to the raw experimental data to determine the true inelastic scattering cross section. The major point-to-point systematic errors in the cross section resulted from an uncertainty in the magnitude of the corrections. These errors were added in quadrature to determine the total uncertainties which are tabulated with the cross sections.

A subtraction for target-empty events was determined by taking otherwise identical data runs with the target emptied of liquid hydrogen. As already noted, this effect varied from 9 to 35% with an uncertainty of less than 2%. Both target-full and target-empty runs were corrected for accidentals and unrejected background. For phase I of the experiment, the accidentals subtraction was about 1% for pions, 5–10% for kaons and 10–15% for antiprotons. The uncertainty in the subtraction ranged from <1 to 5%. For phases II and III the accidentals subtraction was always less than 1%. The subtraction for unrejected background due to Cherenkov-counter inefficiency was less than (25 ± 2)% for K^- data points, approximately (50 ± 10)% for K^+ and $\bar{p}$, and essentially zero for pions and protons.

The number of events was corrected for nuclear interactions of the scattered particle in the upstream stages of the spectrometer, for multiple Coulomb scattering and for the decay of π's and K's. The magnitude and uncertainties in these corrections for each phase of the experiment are listed in Table IV. We determined the absorption corrections from standard interaction length tables (interaction lengths were multiplied by 1.33 for π's and K's). We included an estimation of the probability that an absorptive interaction would produce a particle which would reach the end of the spectrometer. A Monte Carlo computer program computed the correction for particle decay. It simulated the decay of pions and kaons isotropically in the particle rest frame; the decay products were then followed to determine whether they would reach the S_5 counter. A Monte Carlo program was also used to determine the effects of multiple Coulomb scattering in the spectrometer; the program used a Gaussian approximation for the scattering angle distribution.

The singles rates in all counters were low enough so that the correction for discriminator deadtime effects was <1%. There were also no point-to-point uncertainties resulting from misalignment of the apparatus, since none of the counters or magnets were moved during each phase of the experiment.

The over-all normalization uncertainty was approximately 5% as a result of imprecise knowledge of the spallation cross sections. There was an additional point-to-point normalization error from the effect of the fringe

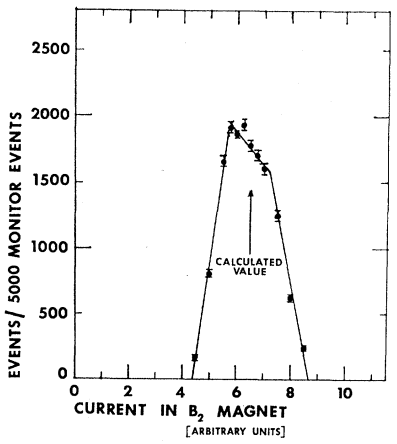

FIG. 12. Plot of the number of events as a function of the B_2 magnet current while the B_1-magnet current is held fixed.

TABLE V. Center-of-mass production cross sections for production of $\pi^{\pm}$ in 12.4–12.5-GeV/c proton-proton collisions as a function of $p_{\perp}^2$.

Particle	$p_l^{\text{c.m.}}$ (GeV/c)	$p_{\perp}^2$ (GeV/c)^2	$(\Delta\Omega\Delta p)_{\text{c.m.}}$ (10^{-6} sr GeV/c)	$(d^2\sigma/d\Omega dp)_{\text{c.m.}}$ [μb/(sr GeV/c)]	Error in $(d^2\sigma/d\Omega dp)_{\text{c.m.}}$ ($\pm$%)
π^-	0.60	0.00	6.90	5980	11
		0.02	6.84	4370	10
		0.04	6.83	3590	9
		0.07	6.82	3040	8
		0.09	6.82	2620	7
		0.11	6.82	2190	6
		0.21	6.88	1250	6
		0.31	6.96	850	5
		0.42	7.06	571	5
		0.52	7.17	378	5
		0.62	7.28	261	5
		0.72	7.39	183	5
		0.82	7.50	123	6
		0.93	7.61	91.4	6
		1.00	9.68	76.8	5
		1.03	7.72	64.0	6
		1.13	7.83	47.0	6
		1.20	9.91	42.0	5
		1.23	7.94	32.3	6
		1.34	8.04	25.8	6
		1.40	10.1	23.0	5
		1.44	8.15	18.0	7
		1.60	10.3	12.4	5
		1.80	10.5	6.98	5
		2.0	10.8	3.99	5
		2.2	11.0	2.26	5
		2.4	11.2	1.19	5
		2.6	11.4	0.644	6
		2.8	11.6	0.393	6
		3.0	11.7	0.224	6
		3.2	11.9	0.126	7
		3.4	12.1	0.0778	7
		3.6	12.3	0.0370	9
		3.8	12.5	0.0229	11
		4.0	12.6	0.0139	12
π^-	0.40	0.10	3.74	2950	9
		0.20	4.16	1660	6
		0.30	4.25	1080	6
		0.40	4.26	733	6
		0.50	3.75	602	12
		0.60	3.44	445	17
π^+	0.60	0.00	6.90	19 000	7
		0.02	6.84	12 800	7
		0.04	6.83	9550	7
		0.07	6.82	7550	7
		0.09	6.82	6080	7
		0.12	6.82	4890	7
		0.22	6.88	2680	6
		0.33	6.96	1870	6
		0.43	7.06	1290	6
		0.53	7.17	871	6
		0.64	7.28	594	6
		0.74	7.39	396	6
		0.85	7.50	277	6
		0.95	7.61	196	6
		1.00	9.68	166	5
		1.05	7.72	135	6
		1.16	7.83	99.3	6
		1.20	9.91	91.6	5
		1.26	7.94	72.5	6
		1.37	8.04	55.1	6
		1.40	10.1	52.4	5
		1.47	8.15	42.9	6
		1.60	10.3	28.5	5
		1.80	10.5	16.4	5
		2.0	10.8	9.81	5
		2.2	11.0	5.84	5
		2.4	11.2	3.06	5
		2.6	11.4	1.75	5
		2.8	11.6	1.10	5
		3.0	11.7	0.684	5

TABLE V (*continued*)

Particle	$p_l^{c.m.}$ (GeV/c)	$p_\perp^2$ (GeV/c)^2	$(\Delta\Omega\Delta p)_{c.m.}$ (10^{-6} sr GeV/c)	$(d^2\sigma/d\Omega dp)_{c.m.}$ [μb/(sr GeV/c)]	Error in $(d^2\sigma/d\Omega dp)_{c.m.}$ ($\pm$%)
		3.2	10.9	0.395	6
		3.4	12.1	0.232	5
		3.6	12.3	0.138	6
		3.8	12.5	0.0792	8
		4.0	12.6	0.0478	8

TABLE VI. Center-of-mass production cross sections for production of $\pi^\pm$ 12.4–12.5-GeV/c proton-proton collisions as a function of $p_l^{c.m.}$.

Particle	$p_\perp^2$ (GeV/c)^2	$p_l^{c.m.}$ (GeV/c)	$(\Delta\Omega\Delta p)_{c.m.}$ (10^{-6} sr GeV/c)	$(d^2\sigma/d\Omega dp)_{c.m.}$ [μb/(sr GeV/c)]	Error in $(d^2\sigma/d\Omega dp)_{c.m.}$ ($\pm$%)
π^-	0.21	0.21	3.07	1900	11
		0.31	3.95	1820	10
		0.41	4.89	1640	9
		0.51	5.87	1440	8
		0.62	6.88	1230	7
		0.72	7.91	1050	6
		0.82	8.95	899	6
		0.92	10.0	748	5
		1.02	11.0	604	5
		1.12	12.1	499	5
		1.23	13.1	396	5
		1.33	14.2	294	5
		1.43	15.3	186	5
		1.53	16.4	95.9	5
π^-	0.41	0.11	2.82	815	11
		0.21	3.51	796	10
		0.31	4.31	744	9
		0.41	5.18	687	8
		0.52	6.10	625	7
		0.62	7.06	564	6
		0.72	8.05	501	6
		0.82	9.07	407	5
		0.92	10.0	336	5
		1.02	11.1	253	5
π^-	0.43	0.17	4.12	579	13
	0.47	0.31	5.65	516	8
	0.47	0.60	9.12	453	5
	0.49	0.46	7.34	426	6
π^-	1.03	0.22	4.59	100	7
		0.32	5.28	89.3	7
		0.42	6.04	80.0	7
		0.52	6.86	72.8	6
		0.62	7.72	62.2	5
		0.72	8.62	50.6	5
		0.82	9.56	42.4	5
		0.93	10.5	32.1	5
		1.03	11.5	23.0	5
		1.13	12.5	15.3	5
		1.23	13.5	9.36	5
		1.33	14.5	5.39	5
		1.43	15.5	2.67	6
		1.53	16.6	1.15	7
π^+	0.22	0.22	3.07	3400	11
		0.32	3.95	3340	10
		0.42	4.89	3210	9
		0.53	5.87	2940	8
		0.63	6.88	2610	7
		0.73	7.91	2380	6
		0.83	8.95	2070	6
		0.94	10.0	1850	5
		1.04	11.0	1600	5
		1.14	12.1	1380	5
		1.25	13.1	1200	5
		1.35	14.2	977	5

TABLE VI (*continued*)

Particle	p_1^2 (GeV/c^2)	$p_l^{c.m.}$ (GeV/b)	$(\Delta\Omega\Delta p)_{c.m.}$ (10^{-6} sr GeV/c)	$(d^2\sigma/d\Omega dp)_{c.m.}$ [μb/(sr GeV/c)]	Error in $(d^2\sigma/d\Omega dp)_{c.m.}$ ($\pm$%)
		1.45	15.3	767	5
		1.55	16.42	555	5
π^+	0.43	0.13	2.82	1360	11
		0.23	3.51	1370	10
		0.33	4.31	1360	9
		0.43	5.18	1340	8
		0.53	6.10	1330	7
		0.63	7.06	1250	6
		0.73	8.05	1160	6
		0.84	9.07	1020	5
		0.94	10.0	919	5
		1.04	11.1	787	5
π^+	0.43	0.17	4.12	988	13
	0.47	0.31	5.65	946	8
	0.47	0.60	9.12	1038	5
	0.49	0.46	7.34	864	6
π^+	1.06	0.24	4.59	184	7
		0.34	5.28	168	6
		0.44	6.04	159	6
		0.54	6.86	146	6
		0.64	7.72	132	5
		0.74	8.62	121	5
		0.84	9.56	104	5
		0.94	10.5	88.9	5
		1.04	11.5	74.1	5
		1.15	12.5	60.0	5
		1.25	13.5	44.7	5
		1.35	14.5	32.4	5
		1.45	15.5	21.8	5
		1.56	16.6	15.3	5

TABLE VII. Center-of-mass production cross sections for production of $K^\pm$ and $\bar{p}$ in 12.5-GeV/c proton-proton collisions.

Particle	$p_l^{c.m.}$ (GeV/c)	p_1^2 (GeV/c)^2	$(\Delta\Omega\Delta p)_{c.m.}$ (10^{-6} sr GeV/c)	$(d^2\sigma/d\Omega dp)_{c.m.}$ [μb/(sr GeV/c)]	Error in $(d^2\sigma/d\Omega dp)_{c.m.}$ ($\pm$%)
K^-	0.6	0.3	7.57	18.5	11
		0.4	7.85	12.2	11
		0.5	7.74	9.2	11
		0.6	7.68	5.7	14
		0.7	7.64	4.0	14
		0.8	7.63	2.4	15
		0.9	7.62	1.38	16
		1.0	7.63	1.24	17
		1.1	7.22	1.17	17
		1.2	6.80	0.98	20
		1.3	6.53	0.66	28
K^-	0.3	0.4	5.06	15.1	13
	0.4		6.24	15.6	11
	0.5		7.05	11.6	11
	0.6		7.85	12.2	14
	0.7		8.33	8.0	12
	0.8		8.16	8.7	13
K^+	0.6	0.3	7.57	154	15
		1.4	11.5	4.9	30
		1.6	11.6	3.1	30
		2.0	11.9	1.0	45
K^+	0.3	0.4	5.16	79	18
	0.4		6.24	89	18
	0.5		7.05	97	27
$\bar{p}$	0.6	0.4	12.2	0.19	40
		0.5	12.6	0.12	60

TABLE VIII. Center-of-mass inelastic scattering cross sections for scattering of protons in 12.4–12.5-BeV/c proton-proton collisions.

$\Delta E_{c.m.}$ (GeV)	$p_{c.m.}$ (GeV/c)	$\theta_{c.m.}$ (deg)	$p_\perp{}^2$ (GeV/c)^2	$(\Delta\Omega\Delta p)_{c.m.}$ (10^{-6} sr GeV/c)	$(d^2\sigma/d\Omega dp)_{c.m.}$ [μb/(sr GeV/c)]	Error in $(d^2\sigma/d\Omega dp)_{c.m.}$ ($\pm$%)
1.47	0.42	2	0.00	18.2	1920	7
		13	0.01	17.8	1400	7
		30	0.05	16.7	1180	7
		44	0.09	15.1	978	7
		58	0.13	13.1	799	7
		72	0.16	11.0	643	8
		87	0.17	8.95	605	9
1.37	0.64	2	0.00	23.7	5070	6
		12	0.02	23.3	3780	6
		21	0.05	22.5	2920	6
		30	0.11	21.3	2310	6
		39	0.17	19.7	1780	6
		48	0.23	17.9	1290	7
		58	0.29	15.9	991	7
		67	0.34	13.8	779	7
		77	0.37	11.7	625	7
		86	0.38	9.78	582	8
1.10	1.05	11	0.04	20.2	11 400	6
		16	0.09	19.8	8940	6
		21	0.14	19.3	6500	6
		25	0.21	18.8	4880	6
		30	0.28	18.1	3800	6
		35	0.37	17.4	2850	6
		40	0.45	16.6	2110	6
		44	0.54	15.7	1520	6
		49	0.63	14.8	1110	6
		54	0.72	13.8	814	6
		58	0.80	12.8	586	6
		63	0.87	11.9	465	6
		68	0.93	10.9	376	6
		73	0.98	9.94	325	6
		78	1.02	8.99	284	7
		82	1.03	8.08	266	7
		87	1.04	7.20	249	8
0.95	1.24	16	0.11	11.2	11 700	6
		21	0.19	11.0	7600	6
		25	0.28	10.6	5180	6
		30	0.39	10.2	3640	6
		35	0.51	9.86	2490	6
		40	0.63	9.38	1690	6
		45	0.76	8.88	1080	6
		50	0.89	8.34	714	6
		54	1.01	7.79	486	6
		59	1.13	7.22	350	6
		64	1.23	6.65	253	6
		69	1.32	6.08	210	6
		74	1.39	5.52	175	6
0.83	1.40	63	1.56	16.0	138	5
		70	1.73	14.0	93.6	5
		76	1.85	12.2	65.6	5
		80	1.90	11.2	57.4	5
0.77	1.46	17	0.18	21.1	10 900	6
		21	0.27	20.7	7060	6
		24	0.37	20.2	4400	6
		28	0.48	19.6	2970	6
		32	0.61	19.0	2080	6
		36	0.74	18.3	1420	6
		40	0.88	17.5	942	6
		44	1.02	16.8	615	6
		47	1.16	15.9	400	6
		51	1.30	15.1	272	6
		55	1.43	14.3	191	6
		59	1.55	13.4	144	6
		63	1.67	12.5	114	6
0.41	1.87	21	0.44	23.3	4400	6
		24	0.60	22.7	2340	6
		28	0.79	22.0	1280	6
		32	1.00	21.3	725	6
		36	1.21	20.5	403	6
		40	1.44	19.7	208	6
		44	1.67	18.8	113	6
		47	1.90	17.8	64.3	6

TABLE VIII (*continued*)

$\Delta E_{c.m.}$ (GeV)	$p_{c.m.}$ (GeV/c)	$\theta_{c.m.}$ (GeV/c)^2	p_1^2 (GeV/c)^2	$(\Delta\Omega\Delta p)_{c.m.}$ (10^{-6} sr GeV/c)	$(d^2\sigma/d\Omega dp)_{c.m.}$ [μb/(sr GeV/c)]	Error in $(d^2\sigma/d\Omega dp)_{c.m.}$ ($\pm$%)
		50	2.13	16.9	39.4	6
		55	2.35	15.9	25.4	6
		57	2.45	15.4	21.4	6
0.29	2.01	21	0.50	24.2	3390	6
		24	0.69	23.5	1610	6
		28	0.91	22.9	857	6
		32	1.14	22.1	432	6
		36	1.40	21.3	215	6
		40	1.66	20.4	104	6
		44	1.93	19.5	54.2	6
		48	2.20	18.5	27.8	6
		52	2.47	17.5	15.4	7
		56	2.72	16.5	10.3	7
0.20	2.10	62	3.43	19.8	5.32	5
		65	3.62	18.7	3.43	5
		70	3.89	16.8	1.93	5
		72	3.99	16.0	1.42	5
		80	4.28	13.3	0.795	6
0.13	2.18	22	0.69	25.3	2550	6
		24	0.81	25.0	1630	6
		26	0.93	24.6	1030	6
		28	1.07	24.2	636	6
		30	1.20	23.8	389	6
		32	1.34	23.4	232	6
		34	1.49	23.0	144	6
		36	1.64	22.5	93.5	6
		38	1.79	22.1	58.2	6
		40	1.95	21.6	38.1	6
		42	2.10	21.1	27.9	6
		44	2.26	20.6	19.0	6
		46	2.42	20.1	13.8	6
		48	2.58	19.6	9.82	6
		49	2.73	19.0	8.04	6
		51	2.89	18.5	5.69	7
		53	3.04	18.0	4.53	7

field of the C magnet on the monitor counters; the magnitude of this effect, which was determined experimentally, was less than 5% with an uncertainty of 2% or less.

The statistical errors ranged from 1 to 10% for the pion data, 3 to 25% for the kaon data, and were as high as 50% for the antiproton cross sections. The largest statistical errors were for the points at large transverse momenta, which had a small cross section and thus a low counting rate.

B. Calculation of Cross Section

The differential cross section in the c.m. frame was calculated using the equation

$$\left.\frac{d^2\sigma}{d\Omega dp}\right|_{c.m.} = \frac{\text{corrected no. of events}}{I_0(N_0\rho t)\Delta\Omega\Delta p}, \qquad (5)$$

where I_0 is the number of incident protons measured by the monitor counters, N_0 is Avogadro's number 6.02×10^{23}, ρ is the density of liquid hydrogen taken as 0.07 g/cm^3, t is the target length, and $\Delta\Omega\Delta p$ is the phase-space volume in the c.m. frame.

The calculated cross sections are listed in Tables V–VIII as a function of c.m. parameters. The errors given include all systematic and statistical effects added in quadrature, but do not include an over-all normalization uncertainty of 5%.

IV. DISCUSSION

The importance of inelastic scattering stems not only from its domination of the total cross section, but also from the possibility that inelastic scattering may, in some sense, drive the elastic scattering. In terms of a simple optical analogy, the diffraction scattering of light from a black disk is caused by the absorption of a portion of the incoming wave by the disk. The occurrence of elastic diffractive scattering as a result of absorption is a straightforward application of the unitarity principle. Since, at least for small momentum transfer, proton-proton elastic scattering is primarily diffractive, there may be some simple relationship between the elastic and inelastic cross sections. One of us (A. D. K.) has proposed a particular model for that relationship[12]; the initial motivation for this series of

[12] A. D. Krisch, Phys. Rev. **135**, B1456 (1964); in *Lectures in Theoretical Physics*, edited by W. E. Brittin *et al.* (Colorado U. P., Boulder, Colo., 1966), Vol. IX. See also J. J. J. Kokkedee and L. VanHove, Phys. Letters **25B**, 228 (1968).

experiments was an attempt to determine whether that particular formulation or any other simple model might relate elastic and inelastic scattering. Since earlier experiments indicated no clear relationship for the cross sections in the laboratory frame, we have measured the inelastic cross sections in the c.m. frame in the expectation that the symmetry of this frame would more clearly reveal the interesting features of the scattering process.

The cross section which we measured, $d^2\sigma/d\Omega dp$ for the production of a single particle, sums over a number of individual channels. For example, when we measure the cross section for the reaction

$$p+p\rightarrow\pi^+ + \text{anything}, \tag{6}$$

we sum over reactions such as

$$\begin{aligned} &p+p\rightarrow p+n+\pi^+,\\ &p+p\rightarrow p+p+\pi^+ +\pi^-,\\ &p+p\rightarrow p+n+\pi^+ +\pi^0, \end{aligned} \tag{7}$$

in addition to many others. There is no attempt made to detect the other final-state particles; any knowledge about these particles implies measuring a higher-order cross section. We have thus adopted a statistical approach, assuming that simplicity lies not in the details of each particular channel but rather in the average behavior. This assumption is possibly reasonable because the inelastic cross section $d^2\sigma/d\Omega dp$ depends only on three variables, p_0 and the p and θ of the scattered particle, while higher-order cross sections depend on so many variables that an intuitive understanding is clearly difficult. Since all phases of the experiment were done at essentially the same incident momentum, we have only investigated the dependence of the cross section on the two parameters of the scattered particle (p and θ).[13] The single energy also did not allow us to see if $d^2\sigma/d\Omega dp$ is the most interesting form of the cross section or if we should consider other forms such as $d^2\sigma/2\pi p_\perp dp_\perp dp_\epsilon$.

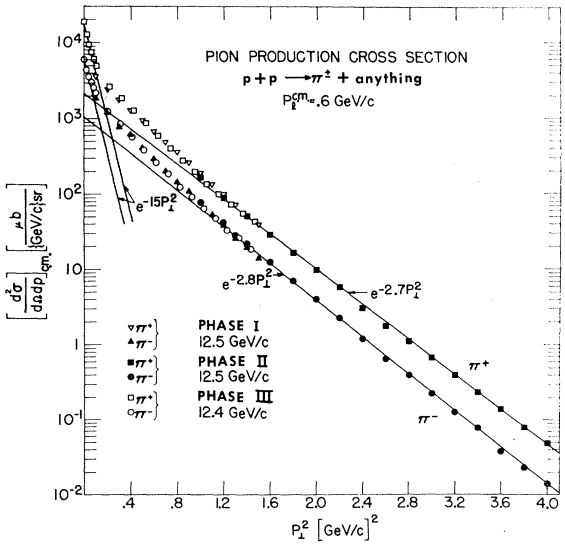

FIG. 13. Plot of $d^2\sigma/d\Omega dp$ for production of $\pi^\pm$ against $p_\perp{}^2$ with $p_l{}^{\text{c.m.}}$ held fixed. The lines are straight-line fits to the data.

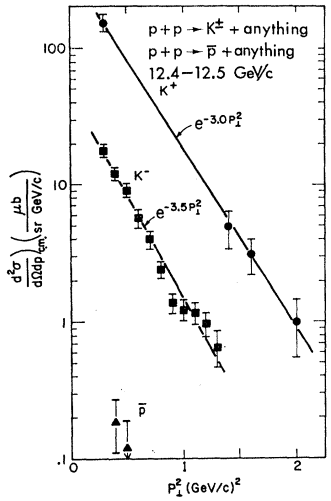

FIG. 14. Plot of $d^2\sigma/d\Omega dp$ for production of $K^\pm$ and $\bar{p}$ as a function of $p_\perp{}^2$ with $p_l{}^{\text{c.m.}}$ held fixed. The lines are straight-line fits to the data.

This production cross section has the additional advantage that it will not vanish as one does experiments at higher c.m. energies, where many believe that the scattering problem may be less complex. Since the total cross section remains approximately constant while the number of open inelastic channels increases with energy, the cross sections for many of these channels must tend to vanish. The doubly-differential cross section sums over an increasing number of reactions as the energy increases, so that the vanishing of the cross section for each channel does not imply that the sum goes to zero. The exact behavior of $d^2\sigma/d\Omega dp$ with increasing energy depends on the energy dependence of the multiplicity of each channel.

Thus it appears that as we go to higher energies, the study of inelastic cross sections of this general type will become increasingly important. The wisdom of our particular choice of c.m. cross sections and parameters will depend on whether the cross sections are simple functions of these parameters. Hopefully this will become more clear as more experiments are done at higher energies.

The detailed discussion of the data can be divided into two portions—the production cross sections for pions, kaons, and antiprotons, and the inelastic scattering cross section for protons.

A. Particle Production Cross Sections

Experiments on proton-proton elastic scattering have shown that the cross section can be well approximated

[13] There is also a third variable φ, the azimuthal angle. However, in an experiment with an unpolarized target and unpolarized beam, the cross section cannot depend on φ.

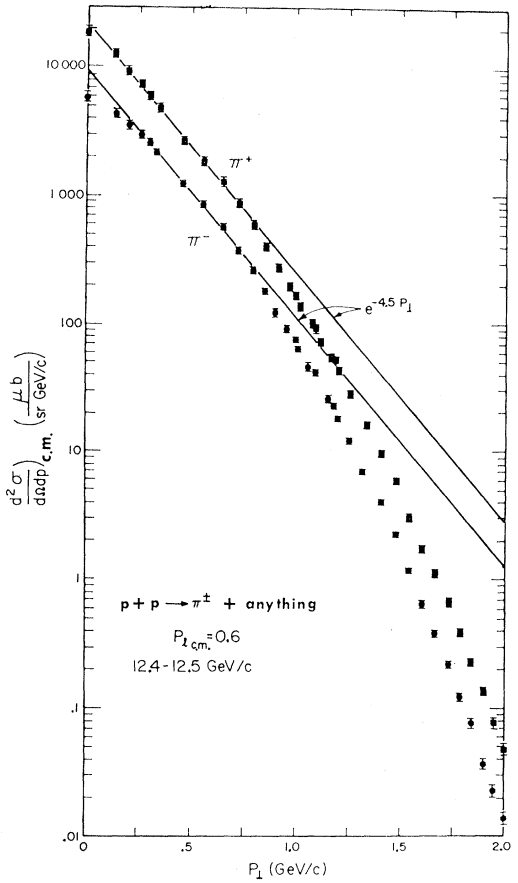

FIG. 15. Plot of $d^3\sigma/d\Omega dp$ for production of $\pi^\pm$ against $p_\perp$ with $p_\parallel^{c.m.}$ held fixed. Notice that the cross section does not seem exponential in $p_\perp$. Compare with the Gaussian dependence shown in Fig. 13.

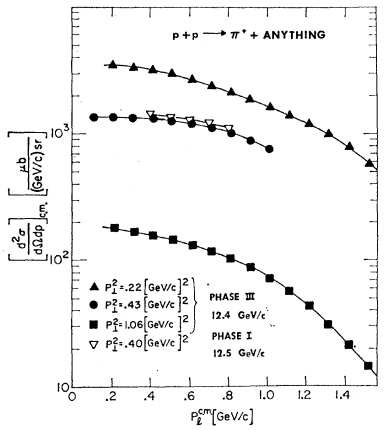

FIG. 16. Plot of $d^3\sigma/d\Omega dp$ for production of π^+ against $p_\parallel^{c.m.}$ with $p_\perp$ held fixed.

by a sum of three Gaussians in the transverse momentum.[14,15] This striking behavior in the elastic cross section, with sharp "breaks" in a semilogarithmic plot of the cross section against $p_\perp^2$, suggests that the inelastic cross section might also show a unique dependence on $p_\perp^2$. The pion production data, shown in Fig. 13, indicate that the inelastic cross section also displays a Gaussian dependence, but there are only two regions and the slopes of each bear no simple relation to the slopes of the regions in elastic scattering. The data for production of kaons and antiprotons, shown in Fig. 14, are much less definitive, but combined with the results of other experiments, the production cross sections for these particles show approximately the same Gaussian behavior as the pion cross sections. Indeed, the slopes of the production cross sections for all the various types of particles seem approximately identical, $d^2\sigma/d\Omega dp \sim e^{-3p_\perp^2}$. The cross-section magnitudes are, of course, different. This equality of slopes seems to rule out any naive connection between the various regions of elastic scattering and the production of different types of particles. Indeed the slope of 3 $(\mathrm{GeV}/c)^{-2}$ probably reflects the fact that the range of strong interaction is slightly less than 1 F. But there is no deeper understanding of why the same slope appears in all inelastic interactions.

The most striking effect which we observed is a sharp forward peak in the pion production cross section. In this forward region the cross section goes as

$$\frac{d^2\sigma}{d\Omega dp} \sim \exp(-15p_\perp^2). \tag{8}$$

As previously mentioned, extensive experimental tests seemed to indicate that this peak was not due to any systematic errors. A possible explanation of this effect has been recently proposed by Yen and Berger.[16] They suggest that the forward peak is a kinematic effect of

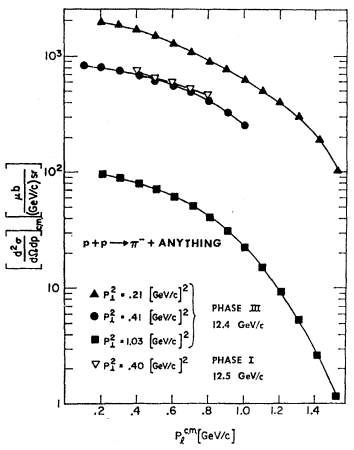

FIG. 17. Plot of $d^3\sigma/d\Omega dp$ for production of π^- against $p_\parallel^{c.m.}$ with $p_\perp$ held fixed.

[14] C. W. Akerlof, R. H. Hieber, A. D. Krisch, K. W. Edwards, L. G. Ratner, and K. Ruddick, Phys. Rev. Letters **17**, 1105 (1966); Phys. Rev. **159**, 1138 (1967); J. V. Allaby, G. Cocconi, A. N. Diddens, A. Klovning, G. Mathtiae, E. J. Sacharidis, and A. M. Wetherell, Phys. Letters **25B**, 152 (1967).

[15] A. D. Krisch, Phys. Rev. Letters **19**, 1149 (1967).

[16] E. Yen and E. Berger, Phys. Rev. Letters **24**, 695 (1970).

pions decaying from low-Q nucleon resonances, so that it could be as sharp as

$$\langle p_\perp{}^\pi\rangle=\langle p_\perp{}^{N^*}\rangle\frac{M_\pi}{M_{N^*}}\approx(400\text{ MeV}/c)\left(\frac{140}{\sim 1400}\right)$$
$$\approx 40\text{ MeV}/c. \quad (9)$$

The nonzero Q value then smears this mean transverse momentum to the observed value of about

$$\langle p_\perp{}^\pi\rangle^{\text{ob}}\approx 200\text{ MeV}/c. \quad (10)$$

Some experimental confirmation of this peak was recently given by a group at CERN, which measured 19.2-GeV/c p-p inelastic scattering.[17] They conclude that their data both are consistent with our suggested behavior

$$\frac{d^2\sigma}{d\Omega dp}=A\exp(-15p_\perp{}^2)+B\exp(-3p_\perp{}^2), \quad (11)$$

and also consistent with a single exponential in $p_\perp$,

$$\frac{d^2\sigma}{d\Omega dp}=C\exp(-6p_\perp). \quad (12)$$

Although the CERN group prefers the exponential parametrization, our data, which extend to $p_\perp=2$ GeV/c, are not consistent with a single exponential. This inconsistency is shown in Fig. 15.

In the paper describing the first section of this experiment, we concluded that the dependence of the production cross section on the c.m. longitudinal momentum p_l was evidence for the existence of two meson-emitting centers or "fireballs" in inelastic interactions. Our present understanding of the previously described difficulties with spectrometer I indicate that there is no evidence for the two-center model. The cross sections measured in later phases of the experiment instead provide some evidence for one-center behavior as is shown in Figs. 16 and 17. Since the two-fireball behavior has possibly been observed in cosmic-ray interactions, we must conclude that the energy of this experiment is still too low to obtain clear separation of the two centers if they exist. At exactly what energy the two centers might finally separate may become evident from planned storage-ring experiments. The p_l dependence of the K-production cross section is shown in Fig. 18 and may be similar to the behavior of the π-production cross section but has larger errors.

The dependence of the production cross section on p_l may be also Gaussian, at least for small p_l, as shown

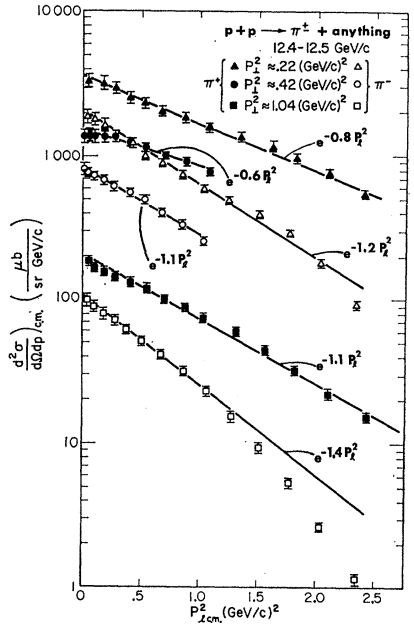

FIG. 19. Plot of $d^2\sigma/d\Omega dp$ for production of $\pi^\pm$ against $(p_l{}^{\text{c.m.}})^2$ with $p_\perp$ held fixed. The lines represent an attempt to fit straight lines to the data.

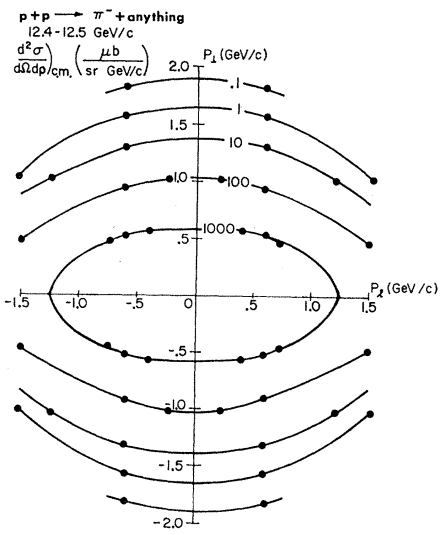

FIG. 20. Contour plot of $d^2\sigma/d\Omega dp$ for production of π^-. The points are interpolated from previous graphs; the lines are a suggestion of the possible shape of the contours.

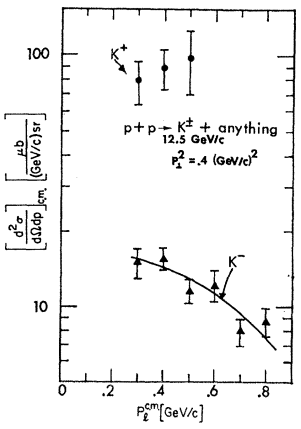

FIG. 18. Plot of $d^2\sigma/d\Omega dp$ for production of K^+ and K^- against $p_l{}^{\text{c.m.}}$ with $p_\perp$ held fixed.

[17] J. V. Allaby *et al.*, CERN report, 1970 (unpublished).

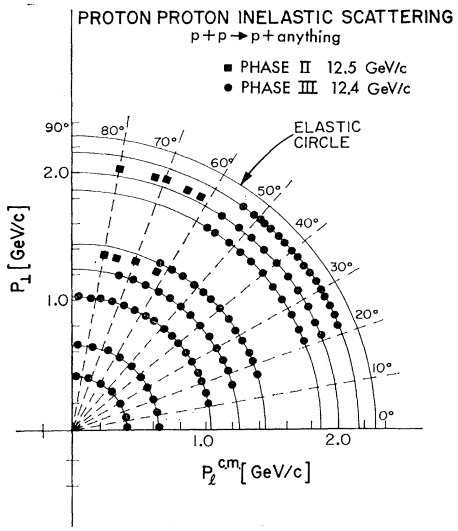

FIG. 21. Center-of-mass plot showing the points at which cross sections were measured for the reaction $p+p \rightarrow p+$anything.

in Fig. 19. The shape, however, is clearly flatter than the $p_\perp$ dependence. The resulting "cigar-shaped" behavior of cross-section contours is shown in Fig. 20. This may be evidence for the suggestion that the particles emerge from a Lorentz-contracted spherical interaction region.[12,18] This would give a cross section whose p_l dependence is flatter than its $p_\perp$ dependence by a factor of γ. At 12.5 GeV/c γ is about 2.6, which might be reasonable. Conclusive tests of this Lorentz flattening must come from additional measurements at other energies.

The behavior in Figs. 16 and 17 is evidence that the c.m. production cross section is "factorable" into functions of the p_l and $p_\perp$ in the c.m. system. That is,

$$\frac{d^2\sigma}{d\Omega dp} = F(p_l)G(p_\perp), \tag{13}$$

where F and G are some functions of their respective variables. This behavior supports the assumption that the c.m. frame is the one in which the cross section is simplest. The recent CERN experiment[17] seems to support this "factorability." The factorability has not yet been tested in the very small $p_\perp^2$ region where the sharp forward peak appears.

B. Inelastic Proton Cross Sections

The cross section for the inelastic scattering of a proton in the reaction

$$p+p \rightarrow p+\text{anything} \tag{14}$$

might be expected to have a simple relationship to elastic scattering. To duplicate the elastic case as closely as possible, we measured the inelastic proton cross section along circles in the c.m. concentric with the elastic circle as shown in Fig. 21. On each circle, $p_{\text{c.m.}}$ is fixed and $\theta_{\text{c.m.}}$ is varied. This was equivalent to holding the missing mass or inelasticity fixed.

We speculated that the relationship between elastic and inelastic scattering might be exhibited through a difference in the inelastic cross section depending on whether only pions or both pions and kaons could be produced.[5] The inelastic circle at $p_{\text{c.m.}}=2.1$ GeV/c is just at threshold for the reaction

$$p+p \rightarrow p+K^+ +\Lambda^0 \tag{15}$$

and below threshold for any other reaction involving strangeness. Figure 22 indicates behavior for this cross section no different than for the cross sections at other inelasticities which allow production of both pions and kaons. This is further evidence against the model that the three regions in pp elastic scattering are due to the production of different particles.[19]

Indeed, the inelastic proton cross section seems relatively independent of inelasticity or missing mass over a large range. This is shown very clearly in Fig. 22. Only for very large inelasticities does the cross section show any dependence on inelasticity. This is similar to the effect first observed by Anderson *et al.*,[1] who found the cross section to be independent of p_l for small $p_\perp$.

The inelastic proton cross section is also Gaussian in $p_\perp$ with a noticeable but less distinct forward peak than in the pion data. The forward peaking is somewhat more clear from a comparison of our data with the small-angle cross sections measured by other groups.[20]

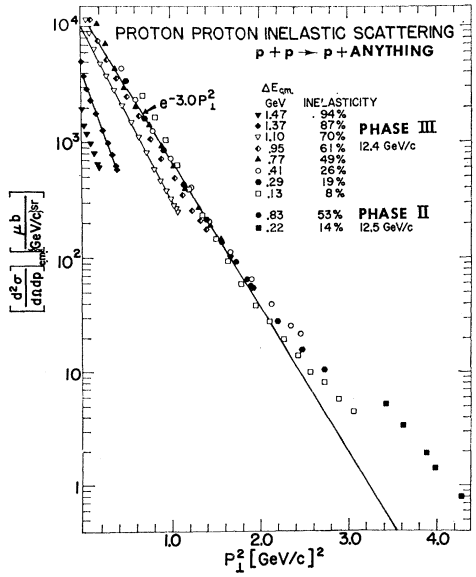

FIG. 22. Plot of $d^2\sigma/d\Omega dp$ for inelastic scattering of protons against $p_\perp^2$ with $\Delta E_{\text{c.m.}}$, the inelasticity, held fixed. This is also equivalent to holding the missing mass fixed.

[18] K. Huang, Phys. Rev. **156**, 1555 (1967).

[19] A recent experiment by Abolins *et al.* [Phys. Rev. Letters **25**, 126 (1970)] shows even more clearly that the second region is not due to kaon production.

The slope of the Gaussian dependence at large $p_\perp$ is approximately 3 $(\mathrm{GeV}/c)^{-2}$,

$$\frac{d^2\sigma}{d\Omega dp} \sim \exp(-3p_\perp^2). \quad (16)$$

In contrast, recently measured deeply inelastic electron data suggest that the extracted inelastic form factors have a very shallow dependence on momentum transfer.[21] The explanation of this apparent difference in behavior awaits further experiments and thought.[22]

It seems likely from our measurements that there are no trivial relationships between proton-proton elastic and inelastic scattering. Because of unitarity, some relationship must exist, but determining this relationship will require some new theoretical analysis using the cross sections which we and other groups have measured.

ACKNOWLEDGMENTS

We would like to thank the entire ZGS staff for their help and encouragement throughout all three phases of the experiment. We also thank Dr. E. Steinberg and the radiochemistry group for their assistance with foil irradiations and Dr. W. F. Baker for his assistance with part of this experiment. We are grateful to Professor D. I. Meyer, Professor M. H. Ross, and Professor K. M. Terwilliger for their helpful comments and suggestions.

[20] See, for example, Anderson *et al.* and Allaby *et al.* (Ref. 1).

[21] E. D. Bloom, D. H. Coward, H. DeStaebler, J. Drees, G. Miller, L. W. Mo, R. E. Taylor, M. Breidenback, J. I. Friedman, G. C. Hartman, and H. W. Kendall, Phys. Rev. Letters **23**, 930 (1969).

[22] The five data points at the largest values of $p_\perp$ seem slightly high in Fig. 22. These points were measured in phase II of the experiment as were several other points which agree well with phase-III cross sections. One possible explanation is that these points include production of the $N^*(1688)$ resonance; another possibility is that there was some contamination from elastic scattering as a result of the relatively large momentum-space bite of the spectrometer. In any case these points are in the resonance region and are not "deeply" inelastic proton-proton scattering.

PHYSICAL REVIEW D VOLUME 3, NUMBER 3 1 FEBRUARY 1971

Nucleon Energy Correlations in the Antineutrino Disintegration of the Deuteron*

CHARLES P. FRAHM†
Argonne National Laboratory, Argonne, Illinois 60439
and
Illinois State University, Normal, Illinois 61761
(Received 7 October 1970)

The correlation in energy between the outgoing nucleons in the process $\bar{\nu}+d \to n+p+\bar{\nu}$ is calculated on the basis of two weak-leptonic–neutral-current models. The results are presented in the form of several graphs. A novel approach to considerations of phase space in the laboratory frame is presented for two-to-three-body processes.

I. INTRODUCTION

RECENTLY, there has been considerable interest in the possible existence or nonexistence of weakly interacting neutral leptonic currents.[1] Although present experimental information tends to cast doubt on the existence of weak neutral leptonic currents, such information, in fact, only argues against certain models involving these currents. The existence of the currents themselves cannot yet be completely ruled out. In fact, the most stringent experimental limitations come from the absence of certain strangeness-changing K decays.[2] These decays, however, are already forbidden if they are governed by a strict $\Delta S=\Delta Q$ rule, independent of the existence or nonexistence of weak neutral leptonic currents. Experiments involving the scattering of neutrinos by nucleons or leptons[3] are free of the $\Delta S \neq \Delta Q$ objection, but place less stringent limitations on the existence of neutral currents. Cundy *et al.* find[4]

$$\sigma(\nu_\mu+p \to \nu_\mu+p)/\sigma(\nu_\mu+n \to p+\mu^-) \leq (0.12\pm 0.06), \quad (1)$$

while Munsee and Reines obtain[5]

$$\sigma(\bar{\nu}_e+d \to p+n+\bar{\nu}_e) < (1.7\pm 1.4)\times 10^{-42}\ \mathrm{cm}^2. \quad (2)$$

* Work performed under the auspices of the U. S. Atomic Energy Commission.

† Permanent address: Illinois State University, Normal, Ill. 61761.

[1] For a recent review of the theoretical and experimental situation, see C. H. Albright and R. J. Oakes, Phys. Rev. D 2, 1883 (1970).

[2] Rolland P. Johnson, LRL Report No. UCRL-19709 (unpublished). A complete list of experimental results is presented in this paper.

[3] F. Reines and H. S. Gurr, Phys. Rev. Letters **24**, 1448 (1970); D. C. Cundy, G. Myatt, F. A. Nezrick, J. B. M. Pattison, D. H. Perkins, C. A. Ramm, W. Venus, and H. W. Wacksmuth, Phys. Letters **31B**, 478 (1970); see also, H. J. Steiner, Phys. Rev. Letters **24**, 746 (1970); C. H. Albright, Phys. Rev. D **2**, 1330 (1970).

[4] D. C. Cundy *et al.*, Ref. 3.

[5] J. H. Munsee and F. Reines, Phys. Rev. **177**, 2002 (1969).